Preprints of the 21st IFAC World Congress (Virtual)
Berlin, Germany, July 12-17, 2020

Elasticity-Aware Online Motion Optimization for Link-Elastic Manipulators

Maximilian Krmer * **Freia I. Muster** * **Christoph Rsmann** *
Torsten Bertram *

* *Institute of Control Theory and Systems Engineering, TU Dortmund University, Dortmund, Germany*
(e-mail: maximilian.kraemer@tu-dortmund.de).

Abstract: The field of human-robot interaction is a typical application of elastic robots, as they reduce the risk of injuries and physical damage in case of a collision. Elasticities, however, also impose high demands on underlying joint controllers to guarantee minimal vibration during regular operation. Numerous control concepts assume a sufficiently high ability to control vibrations, by e.g., dedicated actuators or special kinematic structures. This work presents an online, optimization-based trajectory planning approach that concentrates on maximizing this ability for elastic manipulators without additional damping actuators or certain kinematic structures. The planning algorithm utilizes a modified quadratic objective function to incorporate the *controllability of vibrations* as a secondary goal. The effectiveness of the approach is demonstrated on a real 3-DOF, link-elastic robot for different set-points subject to disturbances. The results show that the approach successfully generates elasticity-aware motions and improves the vibration damping capabilities of the underlying controllers. Especially for critical configurations in which the controllers usually have little or no influence on the vibrations, vibration damping is improved or even made possible.

Keywords: Online Trajectory Planning, Elastic Links, Robotic Manipulators, Model Predictive Control, Vibration Damping.

1. INTRODUCTION

More and more application scenarios for collaborative manipulators emerge in industrial as well as domestic and care applications. The comparatively low potential risk of injuries and physical damage enables fast and flexible operations, which, however, also place additional requirements on trajectory planning. Conventional methods that detect collisions and initiate recovery actions are generally able to fulfill the task but reduce acceptance and efficiency. In contrast, online feedback motion planning introduces a more preventive class of approaches towards collision-free operation in increasingly crowded and changing environments. Still, cases remain where collisions are unavoidable, for example, when the robot is not fast enough to retreat from an obstacle or with increasing uncertainties about the state of the environment. At this point, elastic robots minimize the consequences of collisions and benefits safe physical human-robot interaction.

Elasticities arise from joints (e.g., series elastic actuators) or flexible links. Both convert the kinetic energy into potential energy during collisions but also lead to deflections and vibrations during regular operation, which must be damped using dedicated controllers. Depending on the geometry and actuation of the robot, configurations occur in which vibration damping by the robot's joints is hindered or even infeasible (cf. Tosunoglu et al., 1992). This is especially relevant for robots that do not have dedicated actuators for vibration damping, such as piezoelectric elements. In this context, this article uses the expression *controllability of vibrations* and a corresponding metric for link-elastic robots to describe the ability of a controller to damp vibrations – not to be confused with controllability from control theory. To keep the best possible controllability during operation, this work focuses on considering it at the level of online motion planning.

1.1 Related Work

Model predictive control has proven to be promising for vibration damping as vibrations are predicted and optimized. The prediction model, which describes the relationship between states and controls for joints as well as optional piezo elements, is of particular importance and has been widely studied: The most common approach is to apply the assumed modes method and derive a differential equation that approximates elasticities (Abdolvand and Fatehi, 2012). Elliott et al. (2014) utilize dynamic matrix control as a special type of model predictive control based on step response representation for the prediction model. Dubay et al. (2014) extend this to a model that is based on finite elements to describe elasticities. Since the payload has a considerable influence on the damping behavior of elastic robots, Pradhan and Subudhi (2014); Schnelle and Eberhard (2017) present adaptive approaches to identify model parameters continuously. On the other hand, data-based models such as neural networks are used, for example, by Song and Koivo (1999).

Online trajectory optimization and model predictive control overlap in principle if, in the former, the related

controls are sent instead of the trajectory itself. If the frequency of online planning is sufficiently high, only the most recent control is applied, like in model predictive control. Online trajectory optimization imposes additional requirements on the prediction horizon, collision avoidance, including distance calculations, and other constraints regarding states and controls. The computational complexity of the models above is usually too high for online operation when trajectory planning becomes part of the process. Several approaches plan optimal trajectories for elastic robots offline and pass them to a tracking controller (Esfandiar and Korayem, 2016; Boscariol et al., 2013; Cao and Liu, 2018).

Cascaded approaches finally allow combining online trajectory optimization and vibration damping by separating both problems. The inner cascade linearizes the system behavior and provides vibration damping, while the outer cascade performs online trajectory optimization based on a simplified model. There is a wide range of control concepts for the inner cascade such as state feedback (e.g. Lambeck and Sawodny, 2007) or Lyapunov-based controller (e.g. Reyhanoglu and Hoffman, 2016). As an extension to the classical PID controller, Fareh et al. (2019) use a sliding mode based active disturbance rejection control approach similar to feedback linearization.

1.2 Contribution and Outline

Approaches for vibration damping usually assume sufficient controllability of all vibrations. This assumption is adequate if the robot shows a specific geometry, in which a joint is always able to control the vibration plane of the following link, or additional actuators such as piezoelectric elements are used. Adding more and more linearly independent vibration planes up to an omni-elastic structure for better energy absorption, or merely having a different geometry, controllability is no longer guaranteed by design and might become configuration-dependent. This work aims at maximizing the configuration-dependent controllability introduced by John et al. (2017) and integrates it into an optimization-based approach for elasticity-aware online trajectory planning. The concept follows state of the art by using two cascades, as shown in figure 2. The outer one performs online trajectory optimization, and the inner one carries out vibration damping as well as joint velocity control via a dedicated control concept, which is based on a previous publication by Muster et al. (2019). By elasticity-aware motion planning, vibration damping requires less special kinematic structures and no dedicated actuators. The experimental evaluation focuses on the interaction between both cascades considering a real 3-DOF robot with two elastic links and two intentionally orthogonal vibration planes. The experimental setup is shown in figure 1, highlighting the links' vibration planes in orange and green.

The remainder of this paper is structured as follows. The next section briefly introduces the overall system and the inner cascade with velocity controller and vibration damping. Section 3 introduces the general trajectory optimization problem, which is then specialized for controllability of vibrations and joint space objectives. The results of several real experiments are presented and discussed in section 4. A summary and outlook follow in section 5.

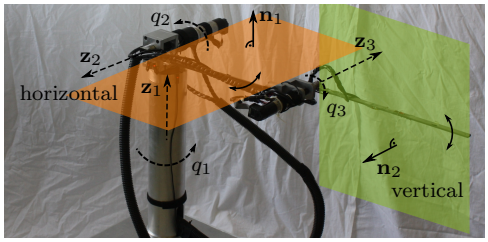

Fig. 1. TUDORA (**TU** **D**ortmund **O**mni-elastic **R**obot **A**dapted) with $N = 3$ DOF and $P = 2$ elastic links in a configuration with maximum controllability.

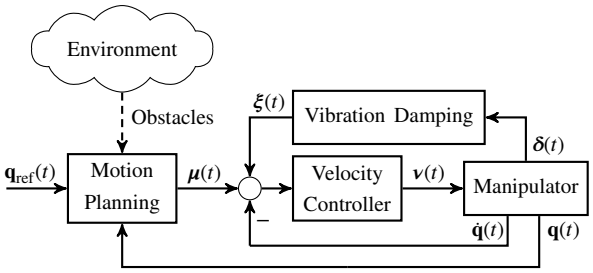

Fig. 2. System and signal overview.

2. VIBRATION DAMPING AND VELOCITY CONTROL

Figure 2 illustrates the inner and outer cascade along with the corresponding signals, giving a general overview of the planning and control system. The inner cascade implements a PI velocity controller based on the actual joint angle velocities $\dot{\mathbf{q}}(t) \in \mathbb{R}^N$ and references $\boldsymbol{\mu}(t) \in \mathbb{R}^N$ for a robot with N joints. For further information on the PI controller design, please refer to Malzahn (2014).

A vibration plane $s_i := (\mathbf{n}_i, \mathbf{t}_i)$ for $i = 1, 2, \ldots, P$ consists of a normal vector $\mathbf{n}_i \in \mathbb{R}^3$ and a point on the plane $\mathbf{t}_i \in \mathbb{R}^3$ with respect to the world frame. It describes the operating range of the additional degrees of freedom of an elastic link due to deflections. Figure 1, for example, shows a 3-DOF robot with two vibration planes highlighted in orange and green.

The velocity feedback $\boldsymbol{\xi}(t) \in \mathbb{R}^N$ for vibration damping is produced based on the zero-mean strain signals $\boldsymbol{\delta}(t) \in \mathbb{R}^P$ on P elastic links, measured by strain gauges or optical strain sensors. Consider $\xi_j : \mathbb{R} \mapsto \mathbb{R}$ as the vibration-related velocity feedback to joint q_j and $j = 1, 2, \ldots, N$:

$$\xi_j(t) = \sum_{i \in \mathcal{I}_j} \delta_i(t)\, k_{j,i}, \tag{1}$$

in which the index set $\mathcal{I}_j \subset \mathbb{N}$ collects all vibration planes s_i that can be controlled by joint q_j. The vibration-related feedback components are lumped together in $\boldsymbol{\xi}(t) \in \mathbb{R}^N$. The proportional gains $k_{j,i} \in \mathbb{R}$ are tuned e.g., by a genetic algorithm during movements around a configuration with the highest controllability of joint j on vibration plane i.

The resulting control outputs $\boldsymbol{\nu}(t) \in \mathbb{R}^N$ correspond to the motor voltages and generate the torques.

3. MOTION PLANNING

Recap figure 2 for the general overview and the interfaces of the outer cascade. The outer cascade receives the

target joint configuration $\mathbf{q}_{\text{ref}}(t)$ for planning. Starting from the current joint configuration $\mathbf{q}(t)$, the outer cascade optimizes an elasticity-aware motion using environmental information like obstacles. This section starts with the general trajectory optimization problem, which is then specialized for controllability and joint space objectives.

3.1 Trajectory Optimization Problem

Trajectory planning in this paper is based on previous work by Krämer et al. (2020) and optimizes a discrete trajectory $\boldsymbol{\tau}_{0:K}$ consisting of $K+1$ joint angles $\mathbf{x}_k \in \mathcal{X}$ and $K \in \mathbb{N}$ joint angle velocities $\mathbf{u}_k \in \mathcal{U}$:

$$\boldsymbol{\tau}_{0:K} \coloneqq \begin{pmatrix} \mathbf{x}_{0:K} \coloneqq \mathbf{x}_0, \mathbf{x}_1, \dots, \mathbf{x}_k, \dots, \mathbf{x}_K \\ \mathbf{u}_{0:K-1} \coloneqq \mathbf{u}_0, \mathbf{u}_1, \dots, \mathbf{u}_k, \dots, \mathbf{u}_{K-1} \end{pmatrix}, \tag{2}$$

with sets $\mathcal{X} \subseteq \mathbb{R}^N$ and $\mathcal{U} \subseteq \mathbb{R}^N$ defining the robot's state space with respect to box constraints:

$$\begin{aligned} \mathcal{X} &\coloneqq \left\{ \mathbf{x} \in \mathbb{R}^N \mid \mathbf{x}_{\min} \leq \mathbf{x} \leq \mathbf{x}_{\max} \right\}, \\ \mathcal{U} &\coloneqq \left\{ \mathbf{u} \in \mathbb{R}^N \mid \mathbf{u}_{\min} \leq \mathbf{u} \leq \mathbf{u}_{\max} \right\}. \end{aligned} \tag{3}$$

By considering joint angles and velocities, most common motion constraints and set-points can be taken into account during planning. The following uniform grid establishes the time law of (2):

$$\begin{aligned} t_0 < t_1 < \ldots < t_k < \ldots < t_K = T, \\ t_{k+1} - t_k = \Delta t. \end{aligned} \tag{4}$$

Both, joint angles $\mathbf{x}_k$ and piecewise constant joint velocities $\mathbf{u}_k$ are introduced as explicit optimization parameters of the nonlinear program:

$$\min_{\substack{\mathbf{u}_{0:K-1}, \\ \mathbf{x}_{0:K}}} \; J(\mathbf{x}_{0:K}, \mathbf{u}_{0:K-1}) \tag{5a}$$

subject to

$$\mathbf{x}_{k+1} - \mathbf{x}_k - \Delta t\, \mathbf{u}_k = \mathbf{0}, \tag{5b}$$
$$\mathbf{u}_k \in \mathcal{U}_{\text{a}}, \tag{5c}$$
$$\mathbf{x}_k \in \mathcal{X}_{\text{c}}(t_k), \tag{5d}$$
$$\mathbf{x}_0 = \mathbf{q}(t_0). \tag{5e}$$

Refer to Nocedal and Wright (2006) for necessary and sufficient optimality conditions.

Expression $J(\cdot)$ in (5a) reflects the overall cost for optimization and is further addressed for planning towards joint space set-points $\mathbf{q}_{\text{ref}}$ in section 3.3. Equality constraint (5b) states the forward-euler difference equation between $\mathbf{x}_k$ and $\mathbf{u}_k$, based on the assumption that the commanded joint velocity sufficiently matches the actual joint velocity. The assumption requires sufficient compensation of cross-couplings via, for example, a centralized control scheme or high gear ratios. In addition, the influence of vibration damping on the respective vibration planes must be ensured, which in turn is part of this approach. Equation (3) already implicitly adds box constraints for $\mathbf{x}_k$ and $\mathbf{u}_k$ to the optimization problem. To also limit joint accelerations, (5c) places additional constraints on $\mathbf{u}_k$:

$$\mathcal{U}_{\text{a}} \coloneqq \left\{ \mathbf{u}_k \in \mathcal{U} \mid \mathbf{a}_{\min} \leq \frac{\mathbf{u}_k - \mathbf{u}_{k-1}}{\Delta t} \leq \mathbf{a}_{\max} \right\}. \tag{6}$$

In case that $k = 0$ the control $\mathbf{u}_{-1}$ equals $\mathbf{u}_0$ of the previous optimization or $\mathbf{0}$ in case of the first run. To avoid collisions, (5d) introduces the set $\mathcal{X}_{\text{c}} \subseteq \mathcal{X}$ that comprises all feasible joint configurations with sufficient clearance between links themselves and obstacles at time t_k. From a practical point of view, (5d) is implemented as inequality constraints for the distances between objects, which are calculated using forward kinematics. For the sake of simplicity, a detailed description of $\mathcal{X}_{\text{c}}$ is not within the focus of this paper.

Consider t_n as closed-loop time instances for $n \in \mathbb{N}_0$, that indicate the n-th trajectory optimization during online planning, with $t_{n+1} - t_n = \Delta t$. By setting t_k for $k = 0$ equal to t_n, and considering (4), the trajectory time t_k starts at the current closed-loop time and consistently extends into the future. This furthermore implies that (5e) ensures that planning starts from the most recent robot joint angle $\mathbf{q}(t_0 = t_n)$. Consider $\mathbf{u}(t)$ as the continuous-time control trajectory of $\mathbf{u}_{0:K-1}$:

$$\mathbf{u}(t) \coloneqq \mathbf{u}_k = \text{const. for } t \in [t_k, t_{k+1}). \tag{7}$$

Then, after each optimization, a portion of the optimal continuous-time control trajectory $\mathbf{u}^\star(t)$ is sent to the inner cascade:

$$\boldsymbol{\mu}\big(\mathbf{q}(t)\big) \coloneqq \mathbf{u}^\star(t)\Big|_{t_0 = t_n} \quad \text{for} \quad t \in [t_n, t_{n+1}). \tag{8}$$

3.2 Controllability of Vibrations

To evaluate the ability of the present joints to dampen vibrations of the robot's elastic links, the configuration-dependent geometric controllability metric introduced by John et al. (2017) is considered. This metric is preferred over others by its less computational burden, the circumvention of deriving a complete dynamic model of the robot, and the unique mapping of each vibration plane to the respective actuator with the most significant influence in the current configuration. This enables time-critical applications such as vibration damping or elasticity-aware motion planning.

Consider the j-th joint with rotation axis $\mathbf{z}_j \in \mathbb{R}^3$ with respect to the world frame, then the controllability of vibrations in plane s_i is worst, if $\mathbf{z}_j^\intercal \mathbf{n}_i = 0$. Conversely, the best controllability is achieved at $|\mathbf{z}_j^\intercal \mathbf{n}_i| = 1$, assuming $|\mathbf{z}_j| = |\mathbf{n}_i| = 1$ without limitation of generality. The function $f_{j,i}(\mathbf{q}) : \mathbb{R}^N \mapsto [0, 1]$ encodes this relationship:

$$f_{j,i}(\mathbf{q}) \coloneqq |\mathbf{z}_j^\intercal(\mathbf{q}) \mathbf{n}_i(\mathbf{q})|, \tag{9}$$

with $f_{j,i}(\mathbf{q})$ inheriting the dependency on $\mathbf{q}$ from forward kinematics to get the rotation axis and normal vector with respect to the world frame. Depending on the kinematic structure of the robot, it may be more convenient to use the angle variant instead:

$$f_{j,i}(\mathbf{q}) \coloneqq |\cos(\theta_{j,i})|, \tag{10}$$

in which $\theta_{j,i} \in \mathbb{R}$ reflects the angle between $\mathbf{z}_j$ and $\mathbf{n}_i$. The geometric controllability matrix $\mathbf{C}(\mathbf{q}) \in \mathbb{R}^{N \times P}$ now captures the influences of all joints (rows) on all vibration planes (columns):

$$\mathbf{C}(\mathbf{q}) \coloneqq \begin{bmatrix} f_{1,1}(\mathbf{q}) & f_{1,2}(\mathbf{q}) & \dots & f_{1,P}(\mathbf{q}) \\ f_{2,1}(\mathbf{q}) & f_{2,2}(\mathbf{q}) & \dots & f_{2,P}(\mathbf{q}) \\ \vdots & \vdots & \ddots & \vdots \\ f_{N,1}(\mathbf{q}) & f_{N,2}(\mathbf{q}) & \dots & f_{N,P}(\mathbf{q}) \end{bmatrix}. \tag{11}$$

The final objective function $c_{\text{C}}(\mathbf{q}) : \mathbb{R} \mapsto [0, NP]$, which is used in the next section for motion planning, is defined as:

$$c_{\mathrm{C}}(\mathbf{q}) \coloneqq \sum_{i=1}^{P} \sum_{j=1}^{N} (1 - f_{j,i}(\mathbf{q})). \tag{12}$$

Maximum controllability $f_{j,i}(\mathbf{q}) = 1 \ \forall \ i, j$, leads to $c_{\mathrm{C}}(\mathbf{q}) = 0$. In the opposite case, $f_{j,i}(\mathbf{q}) = 0 \ \forall \ i, j$ leads to $c_{\mathrm{C}}(\mathbf{q}) = NP$. See section 4.1 for implementation details about a smooth approximation of $|\cdot|$.

3.3 Joint Space Motion Planning

Consider $c_{\mathrm{Q}}(\mathbf{x}) : \mathcal{X} \mapsto \mathbb{R}_0^+$ as the common quadratic objective function to ensure that the trajectory, planned at closed-loop time t_n, tends towards the joint space set-point $\mathbf{x}_{\mathrm{f}} = \mathbf{q}_{\mathrm{ref}}(t_n) \in \mathcal{X}_{\mathrm{c}}$:

$$c_{\mathrm{Q}}(\mathbf{x}) = (\mathbf{x} - \mathbf{x}_{\mathrm{f}})^{\intercal} \, \mathbf{Q} \, (\mathbf{x} - \mathbf{x}_{\mathrm{f}}) \ \text{ for } \mathbf{Q} \in \mathbb{R}^{N \times N}. \tag{13}$$

As stated in section 3.2, the controllability cost $c_{\mathrm{C}}(\mathbf{x})$ also depends on $\mathbf{x}$ (respectively $\mathbf{q}$) and thus generally competes with $c_{\mathrm{Q}}(\mathbf{x})$. Simply adding both terms might result in $\mathbf{x}_{\mathrm{f}}$ not being the actual global minimum anymore, which means never reaching it. When planning offline, one could use an additional final state constraint to force the end of the trajectory to match $\mathbf{x}_{\mathrm{f}}$. However, this is not possible online, since the planning stage only commands the beginning of the control sequence while the constraint merely affects the end.

One possibility to resolve competing objectives online is to fade between them. Time-optimal planning also often utilizes fading to avoid rattling around the set-point. This work considers fading out $c_{\mathrm{C}}(\mathbf{x})$ while $c_{\mathrm{Q}}(\mathbf{x})$ tends to zero:

$$c(\mathbf{x}) = c_{\mathrm{Q}}(\mathbf{x})(\alpha + \beta \, c_{\mathrm{C}}(\mathbf{x})), \tag{14}$$

with weights $\alpha, \beta \in \mathbb{R}^+$. The new objective function $c(\mathbf{x})$ has the following properties:

$$\begin{aligned} &\text{For } c_{\mathrm{Q}}(\mathbf{x}) = 0 \text{ and } c_{\mathrm{C}}(\mathbf{x}) \geq 0 \Rightarrow c(\mathbf{x}) = 0, \\ &\text{For } c_{\mathrm{Q}}(\mathbf{x}) > 0 \text{ and } c_{\mathrm{C}}(\mathbf{x}) \geq 0 \Rightarrow c(\mathbf{x}) \geq c_{\mathrm{Q}}(\mathbf{x}). \end{aligned} \tag{15}$$

In addition to $c(\mathbf{x})$, the overall costs also consider $c_{\mathrm{R}}(\mathbf{u}) : \mathcal{U} \mapsto \mathbb{R}_0^+$ to avoid unnecessary motions, especially in the vicinity of the optimum:

$$c_{\mathrm{R}}(\mathbf{u}) = \mathbf{u}^{\intercal} \mathbf{R} \, \mathbf{u} \text{ for } \mathbf{R} \in \mathbb{R}^{N \times N}. \tag{16}$$

The costs $J(\cdot)$ for joint space set-points are then defined as follows:

$$J(\mathbf{x}_{0:K}, \mathbf{u}_{0:K-1}) \coloneqq \sum_{k=0}^{K-1} c_{\mathrm{R}}(\mathbf{u}_k) + c(\mathbf{x}_k). \tag{17}$$

From (13) and (15) it directly follows that $c(\mathbf{x}) = 0$ only if $\mathbf{x} = \mathbf{x}_{\mathrm{f}}$. The same holds for $c_{\mathrm{R}}(\mathbf{u}) = 0$, if $\mathbf{u} = \mathbf{0}$, which is generally true when $\mathbf{x} = \mathbf{x}_{\mathrm{f}}$ during planning. Although (15) states that $c(\mathbf{x})$ has only one global minimum, it might have several local minima because of $c_{\mathrm{C}}(\mathbf{x})$. These local minima depend on α as well as β. However, α and β also determine the importance of controllability and, therefore, cannot be chosen arbitrarily. Consider the following equilibrium endpoint constraint:

$$\mathbf{x}_K = \mathbf{x}_{\mathrm{f}}, \tag{18}$$

which is added to (5) to enforce asymptotic stability. Assuming zero model mismatch and a sufficiently long horizon K, so that (5) and (18) are fulfilled, it follows from the properties of (17) that the minimum cost of each iteration t_n, decreases in each subsequent iteration t_{n+1} and $\mathbf{x}_{\mathrm{f}}$ is reached (cf. Grüne and Pannek, 2017).

Table 1. Parameters

Parameter	Value	Note
$k_{1,1}$	0.0022	Vibration Damping
$k_{3,2}$	−0.0075	Vibration Damping
$\mathbf{x}_{\max}$	$\begin{pmatrix} 3 & 0.8 & 2.6 \end{pmatrix}^{\intercal}$ rad	
$\mathbf{x}_{\min}$	$\begin{pmatrix} -3 & -4 & -2.6 \end{pmatrix}^{\intercal}$ rad	
$\mathbf{u}_{\max}, \mathbf{u}_{\min}$	$\pm 0.5 \, \mathrm{rad\,s^{-1}}$	Same for all joints
$\mathbf{a}_{\max}, \mathbf{a}_{\min}$	$\pm 1.0 \, \mathrm{rad\,s^{-2}}$	Same for all joints
K	80	Planning Horizon
Δt	0.05 s	
ϵ	0.001	
α	1	
β	1.5	
$\mathbf{Q}$	$\mathrm{diag}(1, 1, 1)$	Diagonal matrix
$\mathbf{R}$	$\mathrm{diag}(1, 1, 1)$	Diagonal matrix

4. EVALUATION

This section introduces the experimental setup and evaluates the results of the experiments for joint space set-points.

4.1 Experimental Setup

Figure 1 shows the robot that is used for experiments. It consists of $N = 3$ joints and two elastic links. Attached strain gauges measure the deflections of the $P = 2$ vibration planes. An additional payload of 300 g is mounted to the end effector. The bounding volumes for collision avoidance are selected in a way that links do not protrude even in case of deflections. For a detailed list of robot parameters, please refer to Muster et al. (2019). Matrix $\mathbf{C}(\mathbf{q})$ for this robot is:

$$\mathbf{C}(\mathbf{q}) = \begin{bmatrix} |\cos(q_2)| & 0 \\ 0 & |\cos(q_3)| \\ 0 & 1 \end{bmatrix}. \tag{19}$$

Since $f_{3,2}(\mathbf{q}) = 1$, the third joint always has sufficient control on the second vibration plane and thus $f_{2,2}(\mathbf{q})$ is neglected in the experiments. This simplifies $c_{\mathrm{C}}(\mathbf{q})$ to:

$$c_{\mathrm{C}}(\mathbf{q}) = 1 - |\cos(q_2)| \approx 1 - \sqrt{\cos^2(q_2) + \epsilon}. \tag{20}$$

Note the approximation of $|\cdot|$ for a small $\epsilon \in \mathbb{R}^+$ to make $c_{\mathrm{C}}(\mathbf{q})$ differentiable for gradient-based solver.

The velocity control loop and vibration damping of section 2 run on a MATLAB®/Simulink® Real-Time™ target with 2 kHz. The motion planner of section 3.1 runs on a computer equipped with an Intel i5-6500 CPU at 3.2 GHz using 8 GB RAM under Ubuntu 16.04. A previously published hypergraph representation encodes the nonlinear optimization problem (5) to exploit sparsity (cf. Rösmann et al., 2018). The optimization problem is solved by the interior point solver IPOpt (Wächter and Biegler, 2006) with a tolerance of 0.001 and up to 25 iterations using the linear solver MA27 from Harwell Subroutine Library (2018). Table 1 summarizes the parameters used for the following experiments. Note, that $\mathbf{Q}$ is the identity matrix, since α and β are used for weighting.

4.2 Experiments

The first three experiments examine the effectiveness of (17) considering the first three pairs of start and target

Table 2. Pairs of start and target configurations

No.	Start Configuration $\mathbf{q}(0)$	Target Configuration $\mathbf{q}_{\mathrm{ref}}(t)$
1	$\left(-\frac{\pi}{2}\ 0\ \frac{\pi}{2}\right)^{\mathsf{T}}$	$\left(\frac{\pi}{2}\ 0\ \frac{\pi}{2}\right)^{\mathsf{T}}$
2	$\left(-\frac{\pi}{2}\ -\frac{\pi}{4}\ \frac{\pi}{2}\right)^{\mathsf{T}}$	$\left(\frac{\pi}{2}\ -\frac{\pi}{4}\ \frac{\pi}{2}\right)^{\mathsf{T}}$
3	$\left(-\frac{\pi}{2}\ -\frac{\pi}{2}\ \frac{\pi}{2}\right)^{\mathsf{T}}$	$\left(\frac{\pi}{2}\ -\frac{\pi}{2}\ \frac{\pi}{2}\right)^{\mathsf{T}}$
4	$\left(-\frac{\pi}{2}\ 0\ 0\right)^{\mathsf{T}}$	$\left(\frac{\pi}{2}\ -\frac{\pi}{2}\ \frac{\pi}{2}\right)^{\mathsf{T}}$

configurations from table 2, respectively. For these set-points, the robot only requires to move the first joint. However, those three pairs differ in the second joint angle to investigate the transition behavior for different levels of controllability. Each pair is performed once without considering controllability (conventional) and once with $c_{\mathrm{C}}(\mathbf{q})$.

Figure 3 shows the controllability $f_{1,1}(\mathbf{q})$ for the first three experiments. In the first experiment (light grey), the controllability is already at its maximum, and both variants do not differ. The second experiment (dark grey) begins and ends with a controllability of 0.7. However, motion planning with $c_{\mathrm{C}}(\mathbf{q})$ (solid) increases controllability temporarily up to almost 1 while it remains static for conventional motion planning (dashed). The same effect appears even stronger in the third experiment (black), for which the robot starts and ends with 0 controllability. Figure 4 shows the joint angle trajectories of this experiment with (solid) and without (dashed) considering controllability. Although the second joint starts at the target value, the modified cost function temporarily deviates it from $-\frac{\pi}{2}$ to increase controllability. The first joint converges directly while the second joint remains on its set-point as they both have no impact on the controllability.

To illustrate the advantage of elasticity-aware planning for vibration damping, the first vibration plane is perturbed by an initial disturbance. Figure 5 shows the measured deflections in the first vibration plane during the disturbed motion of the third experiment with (black) and without (gray) considering controllability. While the deflections are almost identical for both variants during the first second, the amplitudes start decreasing noticeably faster if motion planning takes controllability into account. As can be seen in figure 3 from the solid black line, this is approximately the time at which controllability raises, and the control interventions of vibration damping become more and more effective.

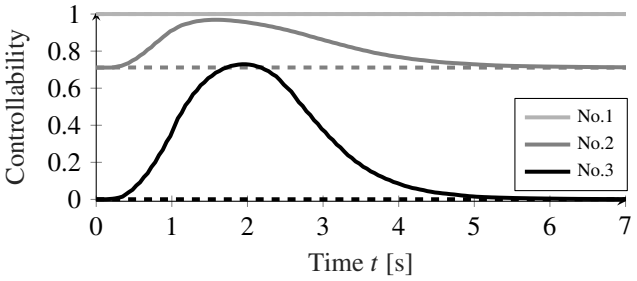

Fig. 3. Controllability $f_{1,1}(\mathbf{q})$ during motion in three different experiments with (solid) and without (dashed) elasticity-aware planning.

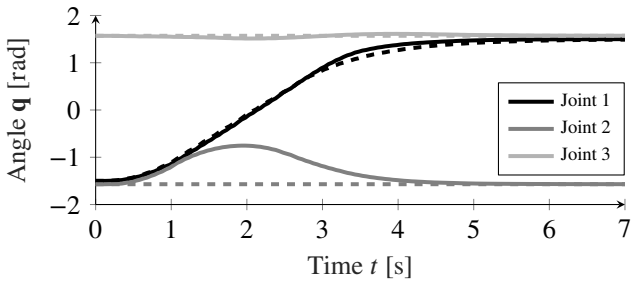

Fig. 4. Joint trajectories of the third experiment with (solid) and without (dashed) elasticity-aware planning.

While during the previous experiments, controllability was equal for start and target configuration, the fourth experiment forces it from 1 to 0. Figure 6 shows the corresponding joint trajectories with (solid) and without (dashed) considering controllability. While the first and the third joint proceed almost identical, there are again differences in the second joint. Through the evaluation of controllability, the motion of the second joint is delayed compared to the conventional case. Additionally, figure 7 illustrates for this experiment how elasticity-aware planning keeps controllability at a higher level for a longer time. This successfully allows vibration damping to be more effective for a longer part of the total motion resulting in better damping performance.

Motion planning takes an average of 19 ms to calculate the next velocity command and therefore has sufficient resources to also react to external influences.

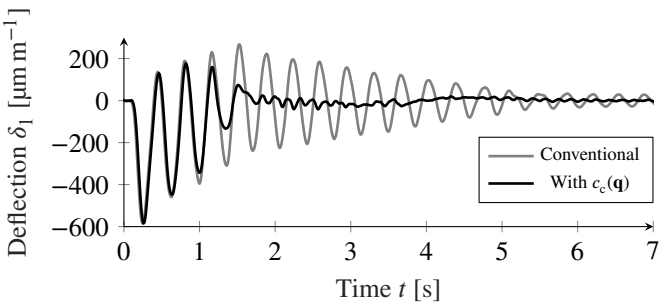

Fig. 5. Deflections in the first vibration plane for an initial disturbance during the third experiment with (black) and without (gray) elasticity-aware planning.

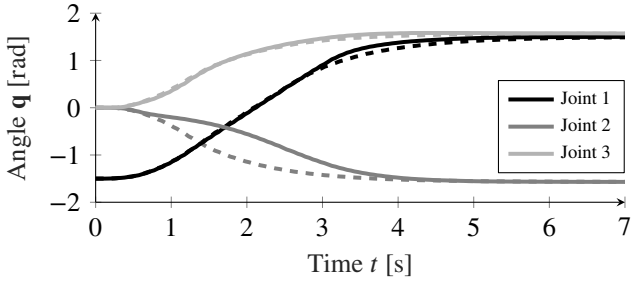

Fig. 6. Joint trajectories of the fourth experiment with (solid) and without (dashed) elasticity-aware planning.

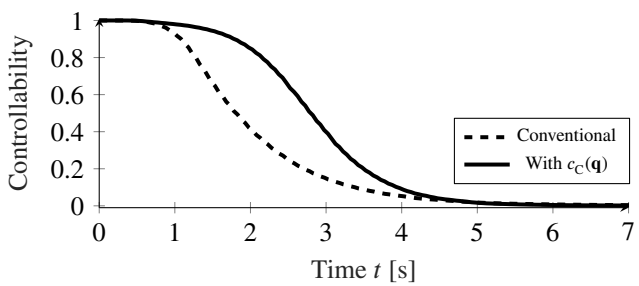

Fig. 7. Controllability of the fourth experiment with (solid) and without (dashed) elasticity-aware planning.

5. CONCLUSION AND OUTLOOK

This paper contributes an online elasticity-aware motion planning approach for link-elastic manipulators, which successfully increases the effectiveness of control interventions for vibration damping by penalizing poor controllability of vibrations. As a result, the amplitudes of vibrations caused by disturbances decay noticeably faster than with conventional planning. The cascaded concept consists of an optimization-based motion planner and a low-level velocity controller, including vibration damping. The effectiveness of vibration damping is quantified by a configuration-dependent metric and optimized during motion planning in the form of a modified quadratic cost function. The results show that even constant components of set-points temporarily deviate in favor of higher controllability. The approach furthermore extends phases of higher controllability for motions towards set-points with poor controllability. Future work will concentrate on the conversion of the equilibrium endpoint constraint into general stabilizing terminal conditions and the introduction of a terminal region to allow shorter planning horizons. Additionally, it is planned to consider an adaptation for β depending on the deflections, to only increase controllability when it is needed.

REFERENCES

Abdolvand, M. and Fatehi, M.H. (2012). Model-base predictive control for vibration suppression of a flexible manipulator. In *International Conference on Control*, 562–567.

Boscariol, P., Gasparetto, A., Vidoni, R., and Romano, A. (2013). A model-based trajectory planning approach for flexible-link mechanisms. In *International Conference on Mechatronics*, 219–224.

Cao, F. and Liu, J. (2018). Optimal trajectory control for a two-link rigid-flexible manipulator with ODE-PDE model. *Optimal Control Applications and Methods*, 39(4), 1515–1529.

Dubay, R., Hassan, M., Li, C., and Charest, M. (2014). Finite element based model predictive control for active vibration suppression of a one-link flexible manipulator. *ISA Transactions*, 53(5), 1609–1619.

Elliott, J.R., Dubay, R., Mohany, A., and Hassan, M. (2014). Model predictive control of vibration in a two flexible link manipulator — Part I. *Journal of Low Frequency Noise, Vibration and Active Control*, 33(4), 455–468.

Esfandiar, H. and Korayem, M.H. (2016). Optimal point to point path planning of flexible manipulator under large deformation by using harmony search method. *Journal of Theoretical and Applied Mechanics*, 179–193.

Fareh, R., Al-Shabi, M., Bettayeb, M., and Ghommam, J. (2019). Robust active disturbance rejection control for flexible link manipulator. *Robotica*, 1–18.

Grüne, L. and Pannek, J. (2017). *Nonlinear model predictive control: Theory and algorithms*. Communications and control engineering. Springer, 2nd edition.

Harwell Subroutine Library (2018). A collection of fortran codes for large scale scientific computation. URL `http://www.hsl.rl.ac.uk/`.

John, F.I., Malzahn, J., and Bertram, T. (2017). Controllability and accessibility of vibrations in multiple planes on link-elastic robot arms. In *ROBIO*, 1491–1496.

Krämer, M., Rösmann, C., Hoffmann, F., and Bertram, T. (2020). Model predictive control of a collaborative manipulator considering dynamic obstacles. *Optimal Control Applications and Methods*.

Lambeck, S. and Sawodny, O. (2007). Trajectory generation and oscillation damping control for a flexible link robot. In *Annual Conference of the Industrial Electronics Society*, 2748–2753.

Malzahn, J. (2014). *Modeling and control of multi-elastic-link robots under gravity*. Ph.D. thesis, TU Dortmund University.

Muster, F.I., Malzahn, J., and Bertram, T. (2019). Exploiting controllability for vibration damping in multiple planes of link-elastic robot arms. In *International Conference on Mechatronics*, 187–192.

Nocedal, J. and Wright, S.J. (2006). *Numerical Optimization*. Springer Series in Operations Research and Financial Engineering. Springer Science, New York, NY, 2nd edition.

Pradhan, S.K. and Subudhi, B. (2014). Nonlinear adaptive model predictive controller for a flexible manipulator: An experimental study. *Transactions on Control Systems Technology*, 22(5), 1754–1768.

Reyhanoglu, M. and Hoffman, D. (2016). Modeling and control of a flexible-structure-mounted manipulator. In *International Conference on Advanced Intelligent Mechatronics*, 953–957.

Rösmann, C., Krämer, M., Makarow, A., Hoffmann, F., and Bertram, T. (2018). Exploiting sparse structures in nonlinear model predictive control with hypergraphs. In *International Conference on Advanced Intelligent Mechatronics*, 1255–1260.

Schnelle, F. and Eberhard, P. (2017). Adaptive nonlinear model predictive control design of a flexible-link manipulator with uncertain parameters. *Acta Mechanica Sinica*, 33(3), 529–542.

Song, B.J. and Koivo, A.J. (1999). Nonlinear predictive control with application to manipulator with flexible forearm. *Transactions on Industrial Electronics*, 46(5), 923–932.

Tosunoglu, S., Lin, S.H., and Tesar, D. (1992). Accessibility and controllability of flexible robotic manipulators. *Journal of Dynamic Systems, Measurement, and Control*, 114(1), 50–58.

Wächter, A. and Biegler, L.T. (2006). On the implementation of an interior-point filter line-search algorithm for large-scale nonlinear programming. *Mathematical programming*, 25–57.